Dipped adcluster model study for molecular and dissociative chemisorptions of O_2 on Ag surface

Hiroshi Nakatsuji and Hiromi Nakai
Department of Synthetic Chemistry, Faculty of Engineering, Kyoto University, Kyoto 606, Japan

(Received 29 October 1991; accepted 23 October 1992)

Chemisorption of an O_2 molecule on a Ag surface is studied theoretically with the use of the dipped adcluster model (DAM). Electron correlations in low-lying surface states and electron-transferred states from bulk metal, which are shown to be very important, are described by the symmetry adapted cluster (SAC)/SAC-configuration interaction (SAC-CI) method. Side-on geometries are used, different from the (bent) end-on geometries studied previously. Potential curves for the O_2 approaching and dissociating processes are investigated with the use of Ag_2O_2 and Ag_4O_2 adclusters. For the occurrence of chemisorption, the electron transfer from bulk metal to the adcluster, and the electrostatic image force are important, which cannot be treated by the conventional cluster model. Two different molecular adsorption states are obtained from the calculations for the Ag_2O_2 adcluster, namely superoxide (O_2^-) and peroxide (O_2^{2-}) species and the corresponding adsorption energies are calculated to be 5.5 and 17.8 kcal/mol, respectively, which compare well with the experimental value 9.2–9.3 kcal/mol. The O–O stretching frequencies of these species are in good agreement with the experimental values. From the calculations for the Ag_4O_2 adcluster, the potential minima corresponding not only to the molecular adsorption, but also to the dissociative adsorption are obtained. The dissociative adsorption is shown to be led from the peroxide. The geometry of the dissociative O^- is at the bridge site on a silver surface and the calculated Ag–O bond distance of 2.16 Å agrees well with the experimental value 2.06–2.17 Å. The dissociative adsorption energy is estimated to be 44.0–61.4 kcal/mol, which is compared with the experimental value 40.8–44.0 kcal/mol.

I. INTRODUCTION

An oxygen molecule chemisorbed on a silver surface shows several important catalytic reactions. In particular, partial oxidation of ethylene[1] is one of the most useful reactions in chemical industry. A lot of studies have been performed for clarifying the nature of the oxygen species adsorbed on a silver surface.

Spectroscopic studies have revealed the existence of at least four adsorbed species; namely, physisorbed species (O_2), molecularly adsorbed species, superoxide (O_2^-) and peroxide (O_2^{2-}), and dissociatively adsorbed species (O^- and/or O^{2-}).[1-12] The physisorbed species on a Ag film at 20 K has the O–O stretching frequency of 1550 cm^{-1} and the O–O distance of 1.24 Å,[1] which are close to those of the free O_2 molecule; $\omega_e = 1580$ cm^{-1} and $R_e = 1.20$ Å.[13] The O–O frequency of the superoxide species was observed at 1053 cm^{-1} (Ref. 2) and that of the peroxide species at 640 (Ref. 2) and 628 cm^{-1} (Ref. 4) on a Ag(110) surface and 697 cm^{-1} (Ref. 2) on a Ag film, which are smaller than those of the peroxide species adsorbed on different metals [790–932 cm^{-1} (Ref. 14)]. The near-edge x-ray adsorption fine structure (NEXAFS) study of O_2/Ag(110) has shown that the O–O axis of these molecularly adsorbed O_2 is parallel to the surface along the $(1\bar{1}0)$ azimuthal axis with the O–O distance of 1.47 ± 0.05 Å.[5] The dissociatively adsorbed oxygen lies on the long bridge site with the O atom situated about 0.2 Å above the Ag(110) surface. The Ag–O distance was observed at 2.06–2.17 Å by the surface extended x-ray adsorption fine structure (SEXAFS) study[12] and the Ag–O vibrational frequency at 325 cm^{-1} by electron energy loss spectroscopy (EELS).[3]

On the theoretical side, some relevant papers[15-21] have been published in recent years. All of these studies use the cluster model. Selmani *et al.*[16] performed local spin density (LSD) calculations for atomic oxygen adsorption on a Ag_4 cluster. They obtained Ag–O distance and vibrational frequency in reasonable accord with the experimental data. McKee[17] studied Ag_2 and Ag_2^+ clusters as models of unpromoted and promoted surfaces. Upton *et al.* calculated the Ag_{24} cluster interacting with O_2 at a long bridge site by the generalized valence bond (GVB) and GVB-CI methods.[18] There, the four Ag atoms at the adsorbate site were described by the 11-electron pseudopotential, while the other 20 Ag atoms were treated by a one-electron pseudopotential. They found that the orientation of O_2 along the $(1\bar{1}0)$ azimuth is preferred to that along the (001) azimuth. Geometric and spectroscopic parameters were in good agreement with the available experimental data. Carter and Goddard examined various postulated pathways for the catalytic epoxidation of ethylene by the GVB and correlation-consistent CI calculations.[19] They used a triangular Ag_3 cluster as a model of a surface and showed the presence of nearly degenerate atomic oxygen species adsorbed on the Ag_3 cluster; one is an oxyradical anion and the other a closed-shell species. They predicted that the former is selective for the olefin epoxidation, but the latter is not.

Some difficult problems still remain in the theoretical studies. One is to describe theoretically both molecular and

 0021-9606/93/032423-14$006.00

dissociative adsorptions and another is to calculate reliable adsorption energy. Actually, no *ab initio* studies have been able to describe the dissociative adsorption of the O_2 molecule on a Ag surface, though recently Panas *et al.* have succeeded in describing the O–O dissociation on a nickel surface.[22] For the molecular adsorption, no reliable adsorption energies have been calculated though several studies have obtained the corresponding potential minimum, as mentioned above. For example, in the GVB/GVB-CI study,[18] the adsorption energy relative to the cluster ground state was calculated to be -14.8 kcal/mol, a negative value, though the energy relative to the cluster excited state was a positive value of 11.1 kcal/mol. Similarly, only the negative adsorption energies have been obtained by the third-order Møller–Plesset (MP3) calculations.[17] Since all of these theoretical studies have used the cluster model, we think that these difficulties are due to the neglect of the effects of the bulk metal in the cluster model calculations.

In this study, we investigate the electronic processes and mechanisms of molecular and dissociative adsorptions of an O_2 molecule on a Ag surface. We use the dipped adcluster model (DAM)[23,24] instead of the cluster model, and include effectively the effects of a bulk metal such as a transfer of electrons of a bulk metal into an admolecule and an image force on a metal surface. For surface electronic processes, electron correlations, roles of lower ground and excited states, and electron transfer are quite important as shown in this and other studies.[25,26] We have separately developed the symmetry adapted cluster (SAC)/SAC-configuration interaction (SAC-CI) method for describing electron correlations in ground, excited, ionized, and electron-attached states of molecules.[27–29] We use this method for calculating lower surface states and electron-transferred surface states from the bulk metal. Some preliminary results have been published.[30]

II. DIPPED ADCLUSTER MODEL

The dipped adcluster model (DAM) has been proposed as a theoretical model for studying chemisorptions and surface reactions involving electron transfers between admolecules and surfaces.[23,24] It was proposed since the conventional cluster model neglects the effect of a bulk metal. The "adcluster" is defined as a combined system of an admolecule and a cluster. It is dipped onto the electron "bath" of a solid metal and an equilibrium is established for electron and/or spin transfers between them. The equilibrium condition is described with the use of the chemical potentials of the adcluster and the solid surface. Namely, at equilibrium, the adcluster is at the min$[E(n)]$ in the range

$$-\frac{\partial E(n)}{\partial n} \geqslant \mu, \tag{1}$$

where $E(n)$ is the energy of the adcluster with n being the number of electrons transferred from the bulk metal to the adcluster and μ is the chemical potential of the electrons of the metal surface. While all the electrons transferred into the admolecule must be supplied by the cluster alone in the conventional cluster model, some of the electrons are supplied from the electron bath of the bulk metal in the DAM.

In the DAM, the bulk orbitals are not considered explicitly—the bulk effect is taken into account only by the above equilibrium condition. This is certainly an approximation, but in this way, we can avoid the "embedding" problem which has certainly many difficulties. Furthermore, we note that the energy of the adcluster is not necessarily the minimum of $E(n)$ as a function of n, as Eq. (1) implies.

The admolecule charged by this electron transfer induces an electrostatic polarization on the metal surface and receives an electrostatic attraction. In the DAM, the energy of the adcluster is given by

$$E=E^{(0)}+E^{(1)}, \tag{2}$$

where $E^{(0)}$ is the electronic energy of the adcluster alone and $E^{(1)}$ is the energy of the electrostatic interaction between the adcluster and the bulk metal.

For $E^{(0)}$, the following molecular orbital (MO) model of the dipped adcluster was proposed:[23] The adcluster is assumed to exchange electrons and spins with the bulk metal through its active MO m, with the other MOs being doubly occupied or completely unoccupied. The energy of the adcluster with n electrons occupying the mth MO is given by

$$E^{(0)}=2\sum_k H_k+\sum_{kl}(2J_{kl}-K_{kl})+n\sum_k(2J_{km}-K_{km}) +nH_m+Q, \tag{3}$$

where k and l run over the doubly occupied MOs. H_k, J_{kl}, and K_{kl} denote the core-Hamiltonian integral, Coulomb repulsion integral, and exchange repulsion integral, respectively. The quantity Q represents the electron repulsion within the active orbital m and depends on the spin coupling. It is given by

$$Q=\|n-1\|J_{mm} \tag{4}$$

for the highest spin coupling and

$$Q=(n/2)^2 J_{mm} \tag{5}$$

for the paired spin coupling.[23] Here, $\|x\|=0$ if $x<0$, $\|x\|=x$ if $0\leqslant x\leqslant 1$, and $\|x\|=1$ if $x>1$. For paramagnetic molecules such as O_2 in the $^3\Sigma_g^-$ state, the potential energy curve calculated by the highest spin coupling connects monotonously with the energy of the separated system, though this is not the case for the paired spin coupling. We, therefore, adopt the highest spin coupling model in the present paper.

In Ref. 23, the electrostatic interaction $E^{(1)}$ is calculated by a localized model. It is expressed by the electrostatic interaction of the charges on the adcluster with the holes located on the nearest-neighbor atoms of the solid. In Ref. 24, this interaction is treated by a delocalized model, i.e., by the method of image force for the complete conductor surface. Since silver has a large conductivity, the delocalized model would be better than the localized one and therefore is adopted here. Of course, in the actual

system, the image charge may be semilocalized, but an inclusion of such effect would cause an ambiguity which is absent in the above two extreme models. In the delocalized model, the image density at the point $\mathbf{x}$ of the surface is given by

$$\sigma(\mathbf{x})=\sum_i \sigma_i(\mathbf{x})=-\sum_i \frac{q_i|\mathbf{a}_i-\mathbf{a}_i'|}{4\pi|\mathbf{a}_i-\mathbf{x}|^3}, \tag{6}$$

where $\mathbf{a}_i$ is the positional vector of the atom A_i and $\mathbf{a}_i'$ is that of the mirror image. For the charge q_i of the atom A_i, we use the Mulliken's atomic charge. The total image force energy E_{if} is calculated by integrating the electrostatic interaction between the charge q_i and the hole $\sigma(\mathbf{x})$ and is given by

$$E_{if}=-\sum_i \sum_j \frac{q_i q_j}{|\mathbf{a}_i-\mathbf{a}_j'|}. \tag{7}$$

The electrostatic interaction within the adcluster should be already included in the energy of the adcluster alone $E^{(0)}$, so that the image force correction term $E^{(1)}$ is estimated by

$$E^{(1)}=E_{if}-E_{in}, \tag{8}$$

where E_{in} is the energy of the electrostatic interaction between the charge q_i and the hole $\sigma(\mathbf{x})$ at the point $\mathbf{x}$ inside the cluster region of the surface, which is estimated by the van der Waals radius of the silver atom 1.70 Å. Clearly, the image force correction $E^{(1)}$ becomes zero as the surface–admolecule separation becomes infinite.

In the present study, we first apply the molecular orbital model of the dipped adcluster to the Ag_2O_2 system and then consider the correlation effects with the use of the SAC/SAC-CI method. We take Ag_2O_2 as an adcluster, in which O_2 interacts with Ag_2 in a side-on bridge form with C_{2v} symmetry. The end-on geometry and the bent ones have been studied separately.[31] The Ag–Ag distance is fixed at 2.8894 Å, which is the equilibrium distance in a solid silver.[32] At an infinite separation, the O_2 molecule is in the $^3\Sigma_g^-$ state and the Ag_2 cluster is in the $^1\Sigma_g^+$ state. The highest (or parallel) spin coupling model is adopted, since it gives a continuous picture leading to a correct separation limit. In the Ag_2O_2 system, the frontier MOs are mainly composed of the π^* MOs of O_2. In the C_{2v} symmetry, the π^* MOs are split into the a_2 and b_1 orbitals, which are parallel and perpendicular to the silver surface, respectively. When n electrons are transferred from the bulk metal to the adcluster, the b_1 MO is occupied by the additional n β-spin electrons because one α-spin electron already occupies this orbital.

The DAM calculations have been performed with the use of the *ab initio* open-shell restricted Hartree–Fock self-consistent-field molecular orbital (RHF-SCF-MO) program. The Gaussian basis set for the silver atom is $(3s3p4d)/[3s2p2d]$ set and the Kr core is replaced by the relativistic effective core potential.[33] For oxygen, we use the $(9s5p)/[4s2p]$ set of Huzinaga–Dunning[34,35] augmented by the diffuse s, p functions of $\alpha=0.059$ as anion bases[36] and the polarization d function of $\alpha=0.30$.

Figure 1 is a display of the $E(n)$ curves, namely, the

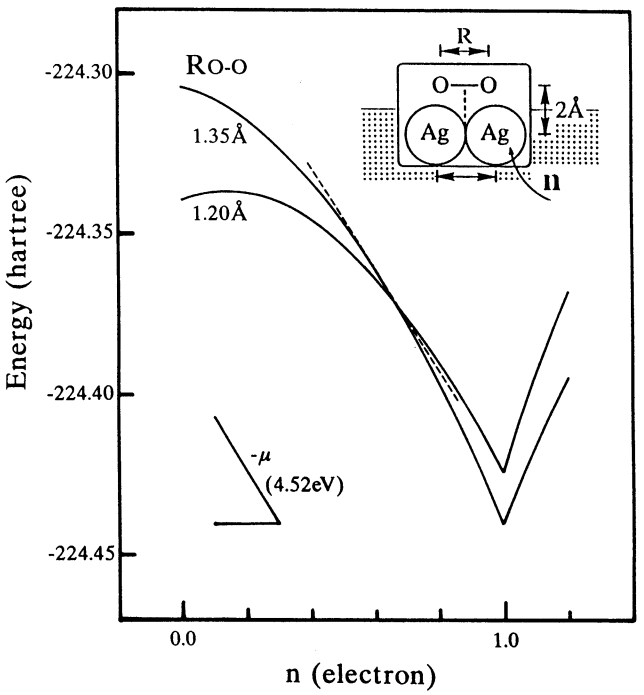

FIG. 1. $E(n)$ curve for the Ag_2O_2 adcluster in the highest spin coupling model with the Ag_2–O_2 distance of 2.00 Å and the Ag–Ag distance of 2.8894 Å. The O–O distance is changed from 1.20 to 1.35 Å.

energy of the adcluster calculated as a function of n. It is calculated by the MO method with the use of the highest spin coupling model.[23] It is for the Ag_2–O_2 distance, the distance between the Ag–Ag axis and the O–O axis, fixed at 2.00 Å. The O–O distance is changed from 1.20 Å, which is an equilibrium length of O_2,[13] to 1.35 Å, which is an equilibrium length for O_2^-.[37] The curves are upper convex and the curvature is discontinuous at $n=0.0$ and $n=1.0$. At $n=0.0$, $R_{O\text{–}O}=1.20$ Å is more stable, but at $n=1.0$, $R_{O\text{–}O}=1.35$ Å is more stable. The tangents of the curves coincide with the experimental chemical potential $-\mu$ of the solid silver metal (4.52 eV) (Ref. 38) at $n=0.6$–0.7. Therefore, as judged from the equilibrium condition of Eq. (1), one electron flows from the bulk metal into the adcluster after some barrier.

We assume that this one-electron flow is valid not only for this molecular orbital model, but also for the cases in which electron correlations are taken into account. We calculate in the next section the correlated wave functions for this one-electron transferred adcluster by the SAC/SAC-CI method.

Last, we note that this one-electron flow is caused by O_2 interacting with the Ag_2 cluster. While the transferred electron mainly occupies the oxygen orbitals, an electron transfer to the Ag_2 cluster will also cause a stabilization by the electron affinity (E.A.) of Ag_2—the experimental value is 1.023 ± 0.007 eV.[39] However, such a stabilization will not bring a situation that the tangent of the $E(n)$ curve coincides with the experimental chemical potential $-\mu$ of the solid silver metal (4.52 eV) such as Fig. 1. Furthermore, without O_2, there is no image force term. Therefore,

TABLE I. Mulliken's atomic charge and the energy partitioning for the Ag_2O_2 adcluster in the O_2 approaching process.[a]

State	$R_{Ag_2-O_2}$ (Å)	Mulliken's atomic charge		Energy of the adcluster alone $E^{(0)}$ (hartree)	Image force correction $E^{(1)}$ (hartree)	Total energy $E^{(0)}+E^{(1)}$ (hartree)
		Ag	O			
$^3B_2$	5.0	+0.003	−0.003	−224.509 02	0.000 00	−224.509 02
(n=0)	4.0	−0.001	+0.001	−224.509 44	0.000 00	−224.509 44
	3.0	−0.027	+0.027	−224.497 88	−0.000 08	−224.497 96
	2.5	−0.060	+0.060	−224.479 12	−0.000 43	−224.479 55
	2.2	−0.073	+0.073	−224.452 19	−0.000 66	−224.452 85
	2.0	−0.081	+0.081	−224.420 69	−0.000 81	−224.421 50
	1.8	−0.028	+0.028	−224.368 67	−0.000 09	−224.368 76
	1.5	+0.009	−0.009	−224.207 75	−0.000 01	−224.207 76
$^3A_2$	5.0	+0.487	−0.487	−224.352 35	−0.020 73	−224.373 08
(n=0)	4.0	+0.480	−0.480	−224.378 77	−0.023 04	−224.401 81
	3.0	+0.411	−0.411	−224.422 04	−0.019 25	−224.441 29
	2.5	+0.344	−0.344	−224.452 07	−0.014 23	−224.466 30
	2.2	+0.314	−0.314	−224.462 30	−0.012 13	−224.474 43
	2.0	+0.290	−0.290	−224.455 24	−0.010 42	−224.465 66
	1.8	+0.235	−0.235	−224.421 83	−0.006 85	−224.428 68
	1.5	+0.124	−0.124	−224.258 77	−0.001 87	−224.260 64
$^2A_2$	5.0	+0.002	−0.502	−224.475 67	−0.021 99	−224.497 66
(n=1)	4.0	−0.008	−0.492	−224.479 77	−0.024 28	−224.504 05
	3.0	−0.058	−0.442	−224.486 62	−0.022 26	−224.508 88
	2.5	−0.141	−0.359	−224.494 08	−0.015 51	−224.509 59
	2.2	−0.184	−0.316	−224.493 42	−0.012 25	−224.505 67
	2.0	−0.234	−0.266	−224.477 52	−0.008 78	−224.486 30
	1.8	−0.286	−0.214	−224.435 60	−0.005 66	−224.441 26
	1.5	−0.410	−0.090	−224.262 51	−0.000 98	−224.263 49

[a]O–O length is fixed at 1.21 Å for the $^3B_2$ state and at 1.35 Å for the $^3A_2$ and $^2A_2$ states.

without O_2, the equilibrium condition of Eq. (1) would not be satisfied.

III. APPROACH OF O_2 ONTO A SILVER SURFACE

We first investigate the potential curve for the approach of an O_2 molecule onto a silver surface. The O_2 molecule approaches in a side-on bridge form to the two Ag atoms in keeping with C_{2v} symmetry. The Ag_2–O_2 distance of the Ag_2O_2 adcluster is changed from 5.0 to 1.5 Å. The O–O distance is fixed at 1.35 Å, though it is optimized at some important geometries.

Electron correlations in the low-lying states of the adcluster are calculated by the SAC/SAC-CI method. Neutral states and one-electron transferred states are calculated and compared to each other. The one-electron transfer from the bulk metal to the adcluster is expressed by calculating the anion states of the neutral adcluster. The active space in the SAC calculation consists of 15 higher occupied orbitals and 25 lower unoccupied orbitals of the neutral adcluster calculated by the HF method. The 15 occupied orbitals are composed mainly of the 4d and 5s atomic orbitals of Ag and the 2p atomic orbitals of O. All single-excitation operators are included in the linked term and double-excitation operators are selected by the second-order perturbation method.[40] For the ground state, double-excitation operators whose perturbation energy with the HF configuration is larger than 5×10^{-5} hartree are included. For the excited, ionized, and electron attached states, the threshold of 5×10^{-5} hartree is used for the second-order energy with one of the main configurations of the excited states.[40] In the SAC/SAC-CI method, triple and quadruple excitations are considered in the unlinked terms as the products of lower excitations. The selections are performed by the method described previously.[40] The HF calculations are carried out with the use of the program GAMESS,[41] and the SAC/SAC-CI calculations are carried out with the program SAC85.[42]

The electrostatic image force correction $E^{(1)}$ is calculated with the use of Mulliken's atomic charges on the oxygens obtained by the SAC/SAC-CI method, which is shown in Table I. Since the system is kept in the C_{2v} symmetry, the charges of the two Ag and two O atoms are equal.

Figure 2 shows the potential energy curves for O_2 approaching onto the silver surface. The ground state of the separated system Ag_2 plus O_2 corresponds to the $^3B_2$ state. The energy of the separated system is estimated by the SAC-CI calculation for the supermolecule with the Ag_2–O_2 distance of 5.0 Å and the O–O distance optimized to be 1.29 Å. The energy is shown by the asterisk in Fig. 2. The energy scale on the right-hand side of Fig. 2 is in kilocalories per molecule relative to the energy of the separated system. The $^3B_2$ state does not involve the electron transfer from the bulk metal to the adcluster, i.e., n=0. As shown in Table I, the Ag and O atoms of the $^3B_2$ state have small charges and therefore the electrostatic energies are very small. Furthermore, the electrostatic energy is almost zero at the region longer than the Ag_2–O_2 distance of 4.0 Å. The

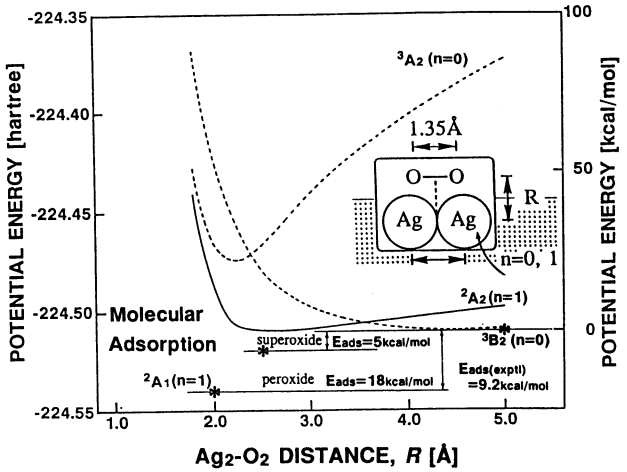

FIG. 2. Potential energy curves for the side-on approach of O_2 onto a silver surface calculated by the SAC/SAC-CI method. The O–O length is fixed at 1.35 Å, while the energies for the optimal O–O lengths are shown by the asterisks. *n* denotes the number of electrons transferred from the bulk metal to the adcluster.

potential energy curve of the $^3B_2$ state rises monotonously as O_2 approaches and shows that O_2 is not adsorbed on the silver surface along this state.

On the other hand, the potential of the $^2A_2$ state is attractive and has a minimum at the Ag_2–O_2 distance of 2.6 Å. The energy of the $^2A_2$ state at the optimal O–O distance of 1.47 Å is shown by an asterisk in Fig. 2. There is another potential minimum at the Ag_2–O_2 distance of 2.0 Å as shown in the next section, and the energy is shown by another asterisk. This is the $^2A_1$ state and is the ground state of the adsorbed system. Both $^2A_2$ and $^2A_1$ states are the adcluster states with one electron transfer from the bulk metal. Since the π^* orbitals of O_2 in the $^2A_2$ and $^2A_1$ states are formally occupied by three and four electrons, respectively, the $^2A_2$ state corresponds to the superoxide species O_2^- and the $^2A_1$ state to the peroxide species O_2^{2-}. The calculated adsorption energies of the superoxide and peroxide species are 5.5 and 17.8 kcal/mol, respectively, in fair agreement with the experimental molecular adsorption energy of 9.2 kcal/mol on Ag(111) and 9.3 kcal/mol on Ag(110).[10] This result shows clearly that the electron transfer from the bulk metal to the adcluster is essentially important for the occurrence of the chemisorption.

The $^3A_2$ state shown in Fig. 2 is an electron transferred state from Ag_2 to O_2, but no electron is supplied from the bulk metal. The potential energy curve of the $^3A_2$ state has a minimum at the Ag_2–O_2 distance of 2.2 Å, but the energy is always higher than that of the separated system. This state corresponds to the superoxide species obtained by the conventional cluster model, though the present potential energy contains the electrostatic energy correction $E^{(1)}$. We see that the adsorption energy is *negative* as in the previous cluster model studies.[17,18] The use of the dipped adcluster model is essential for obtaining positive adsorption energy. It is noted that the atomic charges of O of the $^3A_2$ state are very similar to those of the $^2A_2$ state, while the atomic charges of Ag are not.

The results that the potential energy curves of the $^2A_2$ and $^3A_2$ states have potential minima and that of the $^3B_2$ state is repulsive imply that the electron transfer from the silver surface to O_2 is important for the oxygen chemisorption. Furthermore, the contrasting result of the positive and negative adsorption energies for the chemisorptions along the $^2A_2$ and $^3A_2$ states, respectively, means that the electron transfer from the bulk metal to the adcluster considered by the DAM is essential for describing effectively surface–molecule interactions involving electron transfer within a moderately small computational labor. With the use of the conventional cluster model, the size of the cluster should be much larger than that used here for DAM, since in the cluster model all the electrons transferred to O_2 must be supplied from the cluster, but in DAM, some of the electrons are supplied from the bulk metal.

We now analyze the role of the image force correction term $E^{(1)}$. It increases as the charge of the adsorbate increases and as the distance between the adsorbate and the surface decreases. Furthermore, we note that it decreases as the size of the metal cluster used for the model of the metal surface increases.

Table I shows the atomic charge, the energy of the adcluster alone $E^{(0)}$, the image force correction term $E^{(1)}$, and the total energy for the lower states of the Ag_2O_2 adcluster shown in Fig. 2. For the $^3B_2$ state, which connects with the ground state of the separated system Ag_2+O_2, the oxygen molecule is not much charged and, therefore, the term $E^{(1)}$ is very small. Actually, this term is essentially zero at the Ag_2–O_2 distances of 4.0 and 5.0 Å.

The charges of the Ag and O atoms of the $^3A_2$ state are +0.49 and −0.49, respectively, at the Ag_2–O_2 distance of 5.0 Å, which shows that this state involves one electron transfer from Ag_2 to O_2, while no electron is supplied from the bulk metal. Since the image force is a long-range force which depends on $1/r$, the electrostatic term $E^{(1)}$ amounts to −0.021 hartree even at the large separation of 5.0 Å. As the O_2 molecule approaches the silver surface, the charges of the oxygens decrease by the back donation from O_2 to Ag_2. Therefore, the term $E^{(1)}$ decreases as O_2 approaches Ag_2.

In the $^2A_2$ state, one electron is supplied from the bulk metal to the adcluster. At large separation, the charges of the Ag and O atoms are 0.00 and −0.50, which corresponds to $Ag_2+O_2^-$. Table I shows that the oxygen charge of the $^2A_2$ state is similar to that of the $^3A_2$ state, while the silver charge is not. Since the image force term $E^{(1)}$ depends only on the oxygen charges, the behavior of this term in the $^2A_2$ state is similar to that in the $^3A_2$ state. Therefore, the difference in the total energy between the $^3A_2$ and $^2A_2$ states is due to the difference in the energy $E^{(0)}$ of the adcluster. In the $^3A_2$ state, the electron transferred to O_2 is supplied from the $5s\ \sigma$ MO which contributes to the Ag–Ag bonding, while it is from the bulk metal in the $^2A_2$ state. This is a reason that $E^{(0)}$ of the $^3A_2$ state is higher than that of the $^2A_2$ state in the whole region. At the Ag_2–O_2 distances from 4.0 to 1.5 Å, the Ag atoms of the

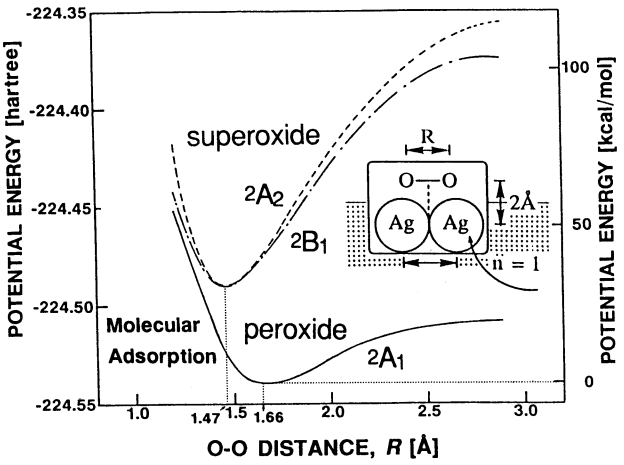

FIG. 3. Potential energy curves for the O–O elongation process in the lowest three states of the Ag_2O_2 adcluster with $n=1$ calculated by the SAC/SAC-CI method. The Ag_2–O_2 length is fixed at 2.00 Å.

$^2A_2$ state are negatively charged, which may show that too many electrons are supplied from the bulk metal. This is perhaps due to the use of the very small cluster such as Ag_2 in the DAM. However, we emphasize here that the conventional cluster model using the small Ag_2 cluster cannot describe the oxygen adsorption on a silver surface, in contrast to the DAM.

IV. THE POTENTIAL CURVE FOR O–O STRETCHING ON A SILVER SURFACE

We next calculate the potential energy curves of O_2 on the silver surface. We study the adsorption states of O_2, their vibrational frequencies, and the dissociative adsorption processes. We first use the Ag_2O_2 adcluster with the Ag–Ag distance fixed at 2.8894 Å. The Ag_2–O_2 distance is fixed at 2.0 Å, which is almost the most stable distance for the adsorbed peroxide state, while the minimum of the superoxide state is at the Ag_2–O_2 distance of 2.6 Å. The O–O distance is elongated from 1.20 to 2.8894 Å in keeping with C_{2v} symmetry. The energy of the adcluster is calculated by the SAC/SAC-CI method. The one-electron transferred states ($n=1$) of the adcluster are calculated as the cation states of the dianion adcluster. The active space consists of 16 higher occupied orbitals and 24 lower unoccupied orbitals of the dianion adcluster calculated by the HF method. The configuration selection thresholds used in the SAC/SAC-CI calculations are the same as those used in the O_2 approaching process.

The potential energy curves for the O–O stretching process are shown in Fig. 3. There are three important states in the lower energy region. Namely, the $^2A_1$ state is the ground state and corresponds to peroxide O_2^{2-}. The $^2A_2$ and $^2B_1$ states are the lower excited states, which are close to each other and correspond to superoxide O_2^-. In the $^2A_2$ state, the in-plane π^* MO of O_2 with the symmetry b_1 is doubly occupied and the out-of-plane π^* MO with the symmetry a_2 is singly occupied. In the $^2B_1$ state, the occupations in the two π^* MOs are reverse.

We summarize in Table II the adsorption energies, geometries, vibrational frequencies, and gross charges calculated for these three oxygen species on the silver surface. As mentioned before, the calculated molecular adsorption energies for the superoxide and peroxide show reasonable agreement with the experimental value. The Ag_2–O_2 distance of the superoxide is calculated to be 2.6 Å and that of the peroxide to be 2.0 Å. This result suggests that the superoxide is first formed, when O_2 approaches silver, due to the one-electron transfer to the π^* MO. The superoxide would then transform easily into the peroxide with a further electron transfer since the latter is more stable than the former by 12 kcal/mol. In this transformation, the Ag_2–O_2 distance changes from 2.6 to 2.0 Å and the bonding between the oxygen species and the silver surface becomes stronger.

The O–O distances of the superoxide and peroxide are calculated to be 1.47 and 1.66 Å, respectively. The calculated value of the O–O distance of the peroxide by Upton *et al.* is 1.55 Å.[18] The NEXAFS experiment showed the distance to be 1.47 ± 0.05 Å.[5] On the other hand, the O–O vibrational frequencies of the superoxide are calculated at 1055 cm^{-1} ($^2A_2$) and 974 cm^{-1} ($^2B_1$) in comparison with the experimental value of 1053 cm^{-1}.[2] For the peroxide species, the theoretical value is 689 cm^{-1} in comparison with the experimental values of 628–697 cm^{-1}.[2–4] The agreement is excellent showing that the present model de-

TABLE II. Adsorption energy, geometry, vibrational frequency, and gross charge of the molecular adsorption species of O_2 on a Ag surface calculated from the Ag_2O_2 adcluster.

Species	State	Adsorption energy (kcal/mol)	Bond length (Å)		O–O vibrational frequency (cm^{-1})	Gross charge (per O_2)
			$R(Ag_2$–$O_2)$	R(O–O)		
Superoxide	$^2A_2$	5.5	2.6	1.47	1055	−0.54
	$^2B_1$	...	...	1.47	974	−0.65
	Exptl.	9.2–9.3[a]	...	...	1053[b]	...
Peroxide	$^2A_1$	17.8	2.0	1.66	689	−1.4
	Exptl.	9.2–9.3[a]	...	1.47±0.05[c]	628–697[d]	...

[a]Reference 10.
[b]Reference 2.
[c]Reference 5.
[d]Reference 2–4.

TABLE III. Mulliken's atomic charge and the energy partitioning for the Ag_2O_2 adcluster in the O–O stretching process.[a]

State	R_{O-O} (Å)	Mulliken's atomic charge		Energy of the adcluster alone $E^{(0)}$ (hartree)	Image force correction $E^{(1)}$ (hartree)	Total energy $E^{(0)}+E^{(1)}$ (hartree)
		Ag	O			
$^2A_1$	1.20	−0.106	−0.394	−224.432 19	−0.019 24	−224.451 43
($n=1$)	1.35	+0.048	−0.548	−224.458 72	−0.037 24	−224.495 96
	1.50	+0.187	−0.687	−224.472 66	−0.058 48	−224.531 14
	1.75	+0.218	−0.718	−224.474 81	−0.063 76	−224.538 57
	2.00	+0.215	−0.715	−224.463 29	−0.063 21	−224.526 50
	2.25	+0.207	−0.707	−224.454 98	−0.061 78	−224.516 76
	2.89	+0.216	−0.716	−224.444 29	−0.063 78	−224.508 07
$^2A_2$	1.20	−0.490	−0.010	−224.417 68	−0.000 01	−224.417 69
($n=1$)	1.35	−0.292	−0.208	−224.473 81	−0.005 38	−224.479 19
	1.50	−0.232	−0.268	−224.480 15	−0.008 91	−224.489 06
	1.75	−0.208	−0.292	−224.449 51	−0.010 52	−224.460 03
	2.00	−0.210	−0.290	−224.412 22	−0.010 39	−224.422 61
	2.25	−0.214	−0.286	−224.383 33	−0.010 07	−224.393 40
	2.89	−0.190	−0.310	−224.344 65	−0.011 93	−224.356 58
$^2B_1$	1.20	−0.230	−0.270	−224.433 83	−0.009 01	−224.442 84
($n=1$)	1.35	−0.206	−0.294	−224.471 13	−0.010 67	−224.481 80
	1.50	−0.174	−0.326	−224.476 17	−0.013 13	−224.489 30
	1.75	−0.147	−0.353	−224.447 85	−0.015 45	−224.463 30
	2.00	−0.132	−0.368	−224.414 23	−0.016 76	−224.430 99
	2.25	−0.086	−0.414	−224.390 88	−0.021 23	−224.412 11
	2.89	−0.106	−0.394	−224.355 10	−0.019 32	−224.374 42

[a]Ag_2–O_2 length is at 2.00 Å.

scribes well the molecular adsorption states of O_2 on a silver surface. As expected, the O–O bond of the peroxide is more relaxed than that of the superoxide.

The atomic charge and the energy partitioning into $E^{(0)}$ and $E^{(1)}$ are shown in Table III. Since the Ag_2–O_2 distance is fixed at 2.0 Å in the O–O stretching process, the image force correction term $E^{(1)}$ is influenced mainly by the oxygen charges. In the peroxide $^2A_1$ state, the gross charge of the oxygen atom changes from −0.39 to −0.72, and the term $E^{(1)}$ from −0.019 to −0.064 hartree. The oxygen charge of the superoxide $^2A_2$ state is similar to, but a little smaller than that of the superoxide $^2B_1$ state. Namely, the oxygen charges are −0.01−−0.31 and −0.27−−0.41 for the $^2A_2$ and $^2B_1$ states, respectively, and the term $E^{(1)}$ from 0.000−−0.012 and −0.009−−0.021 hartree, respectively. Thus, the stabilization due to the image force is larger for the peroxide than for the superoxide. Actually, when the image force correction is ignored, the superoxide is more stable than the peroxide, and furthermore, the adsorption energies of the both species are negative. This result shows that in addition to the electron transfer from the bulk metal to the adcluster, the electrostatic image force is important for stabilizing O_2 on a surface.

The gross charges of the superoxide at the equilibrium geometry are calculated to be −0.54 and −0.65 for the $^2A_2$ and $^2B_1$ states, respectively, and that of the peroxide to be −1.4. Backx *et al.* estimated the charge of −1.7 for the peroxide from the consideration on the vibrational frequency as a function of the number of electrons in the π^* orbitals.[4] It is noted that the atomic charges of Ag at the $^2A_1$ state are positive at the O–O distances between 1.35 and 2.89 Å, while those at the $^2A_2$ and $^2B_1$ states are negative.

V. DISSOCIATIVE ADSORPTION ON A SILVER SURFACE

In the potential curves shown in Fig. 3, there is no minimum corresponding to the dissociative adsorption state—only molecular adsorption states are obtained. The barriers exist around the O–O distance of 2.89 Å for all the states shown. The energy difference between the minimum and the barrier is 20 kcal/mol for the peroxide $^2A_1$ curve, while they are 84 and 72 kcal/mol for the superoxide $^2A_2$ and $^2B_1$ curves, respectively. This result seems to indicate that the dissociative adsorption is led from the peroxide species, though it does not exist in the range of the O–O distance studied here. A reason is attributed to the electrostatic repulsion between the negative charges on the two oxygen atoms. It is estimated as large as 60 kcal/mol from the gross charges on the oxygens (−0.72) separated by 2.89 Å in the $^2A_1$ state. Further separation of the two oxygen atoms on a surface would reduce this repulsion and may lead to the dissociated state. We, therefore, have to investigate a further elongation of the O–O distance on a larger Ag surface.

We therefore undertake to use the *linear* Ag_4 cluster and elongate the O–O distance on this "surface." We carry out calculations for the Ag_4O_2 adcluster with the Ag–Ag and Ag_4–O_2 distances of 2.8894 and 2.0 Å, respectively. The O–O distance is elongated from 1.20 to 8.6682 Å in keeping with C_{2v} symmetry. Based on the results shown in Fig. 1, we calculate one-electron transferred states of the

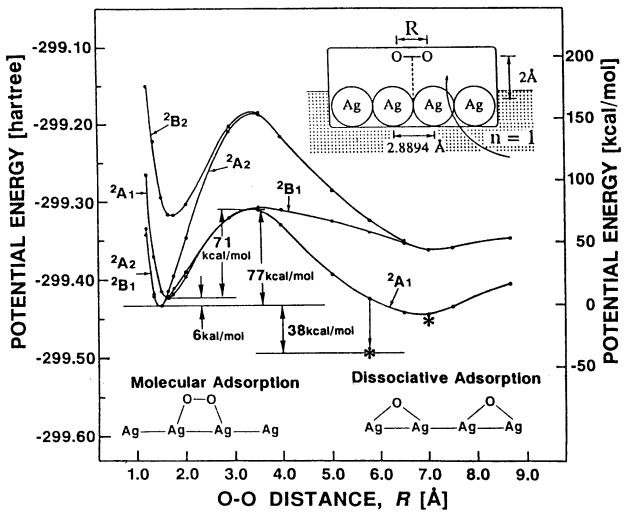

FIG. 4. Potential energy curves for the O–O dissociation process in the lowest three states of the Ag_4O_2 adcluster with $n=1$ calculated by the SAC/SAC-CI method. The Ag_4–O_2 length is fixed at 2.00 Å.

adcluster ($n=1$), which are expressed as the cations of the dianion adcluster in the SAC/SAC-CI method. The active space for the SAC/SAC-CI calculation consists of seven higher occupied orbitals and 81 lower unoccupied orbitals calculated by the HF method. The seven occupied orbitals consist mainly of the 5*s* atomic orbitals of Ag and the 2*p* atomic orbitals of O, which indicates that the 4*d* atomic orbitals of Ag are treated as frozen orbitals. The configuration selection threshold for the linked operators are 5×10^{-5} hartree in the SAC calculation, but no selection is made in the SAC-CI calculations.

The potential energy curves for the low-lying states of the Ag_4O_2 adcluster ($n=1$) for the elongation of the O–O distance are shown in Fig. 4. There are three states $^2A_1$, $^2A_2$, and $^2B_1$ in the lower energy region. The potential minima of these three states exist around the O–O distance of 1.4–1.6 Å and correspond to the molecular adsorption states, the $^2A_1$ state corresponds to the peroxide species, and the $^2A_2$ and $^2B_1$ states correspond to the superoxide species as in the previous case of the Ag_2O_2 adcluster. In Fig. 4, the superoxide species are calculated to be more stable than the peroxide species, in contrast to the results of the Ag_2O_2 adcluster shown in Figs. 2 and 3. We think that the descriptions of these molecularly adsorbed states are more reliable in the calculations of the Ag_2O_2 adcluster than in those for the Ag_4O_2 one, since in the latter calculations, we have neglected the effect of electron correlations of the *d* electrons of the silver cluster.

A remarkable feature of the potential energy curves for the Ag_4O_2 adcluster is that another minimum exists at about $R_{O\text{-}O}=7.0$ Å of the $^2A_1$ state potential curve and it is about 50 kcal/mol lower than those of the $^2A_2$ and $^2B_1$ states. This minimum corresponds to the dissociative adsorption state of O_2 on a silver surface. We further optimize the Ag_4–O_2 distance at the O–O distances of 5.78 and 7.0 Å. The Ag_4–O_2 distance becomes shorter up to 1.60 and 1.90 Å, respectively, and the corresponding energies are shown by the asterisks in Fig. 4. This result shows that the dissociated oxygens are adsorbed at the twofold bridge site of the Ag surface. The large separation of 5.78 Å between the dissociated oxygens is due to the Coulomb repulsion between their negative charges as mentioned before. However, the repulsion still remains at this separation, so that the dissociated oxygens seem to migrate further from the neighboring bridge site to another more distant bridge site. This may be an explanation for the ($m\times1$) low energy electron diffraction (LEED) patterns of the oxygen atoms on the Ag(110) surface, where *m* decreases from 7 to 2 as the oxygen coverage increases.[6] The smallest number $m=2$ corresponds to the bridge site obtained in this study.

The calculated adsorption energy, geometry, and gross charge for the dissociative adsorption state are shown in Table IV and compared with the experimental values. The adsorption energy is estimated to be 61.4 kcal/mol as a sum of the peroxide adsorption energy, calculated from the Ag_2O_2 adcluster, and the energy difference between the peroxide and dissociative species, calculated from the Ag_4O_2 adcluster. By summing the superoxide adsorption energy in the Ag_2O_2 adcluster and the energy difference between the superoxide and dissociative species in the Ag_4O_2 adcluster, the dissociative adsorption energy is calculated to be 44.0 kcal/mol. The thermal desorption spectroscopy (TDS) study of O_2 on Ag(111) and Ag(110) surfaces shows the dissociative adsorption energies of 40.8 and 44.0 kcal/mol, respectively.[10] The agreement between the theoretical and experimental values is better for the latter estimate. We emphasize that this is the first time of theoretically reproducing the dissociative adsorption of O_2 on an Ag surface. The calculated Ag–O distance is 2.16 Å, which agrees well with the observed value of 2.06–2.17

TABLE IV. Adsorption energy, geometry, and gross charge of the dissociative adsorption species of O_2 on a Ag surface calculated from the Ag_4O_2 adcluster.

Method	State	Adsorption energy (kcal/mol)	Bond length (Å)		Gross charge (per O)
			R(Ag–O)	*R*(O–O)	
Theoretical	$^2A_1$	44.0, 61.4	2.16	5.78	−0.98
Experimental		40.8–44.0[a]	2.06–2.17[b]	...	...

[a]Reference 10.
[b]Reference 12.

TABLE V. Mulliken's atomic charge and the energy partitioning for the Ag_4O_2 adcluster in the O–O dissociating process.[a]

State	R_{O-O} (Å)	Mulliken's atomic charge Ag_a[b]	Mulliken's atomic charge Ag_b[b]	Mulliken's atomic charge O	Energy of the adcluster alone $E^{(0)}$ (hartree)	Image force correction $E^{(1)}$ (hartree)	Total energy $E^{(0)}+E^{(1)}$ (hartree)
$^2A_1$	1.20	+0.231	−0.166	−0.566	−299.230 37	−0.035 67	−299.266 04
($n=1$)	1.35	+0.267	−0.089	−0.678	−299.318 98	−0.051 12	−299.370 10
	1.50	+0.261	−0.069	−0.692	−299.361 69	−0.052 94	−299.414 63
	1.65	+0.267	−0.076	−0.692	−299.370 75	−0.052 74	−299.423 49
	1.75	+0.270	−0.080	−0.689	−299.365 42	−0.052 21	−299.417 63
	2.00	+0.283	−0.100	−0.684	−299.345 42	−0.051 02	−299.396 44
	2.89	+0.328	−0.155	−0.672	−299.271 00	−0.047 99	−299.318 99
	4.00	+0.218	+0.002	−0.726	−299.275 97	−0.054 26	−299.330 23
	5.00	+0.058	+0.180	−0.738	−299.338 74	−0.054 77	−299.393 51
	5.78	+0.012	+0.259	−0.771	−299.365 57	−0.058 90	−299.424 47
	5.78*[c]	+0.219	+0.256	−0.975	−299.401 28	−0.091 70	−299.492 98
	6.50	−0.005	+0.293	−0.788	−299.382 59	−0.060 85	−299.443 44
	7.00	−0.003	+0.299	−0.796	−299.382 98	−0.061 77	−299.444 75
	7.00*[c]	+0.002	+0.328	−0.830	−299.389 21	−0.066 90	−299.456 11
	7.50	−0.021	+0.316	−0.796	−299.373 58	−0.061 65	−299.435 23
	8.67	+0.058	+0.235	−0.793	−299.344 43	−0.062 40	−299.406 83
$^2A_2$	1.20	+0.049	−0.319	−0.230	−299.328 72	−0.005 91	−299.334 63
($n=1$)	1.35	+0.069	−0.276	−0.293	−299.411 10	−0.009 52	−299.420 63
	1.50	+0.055	−0.262	−0.293	−299.423 51	−0.009 53	−299.433 04
	1.65	+0.064	−0.265	−0.299	−299.405 17	−0.009 85	−299.415 03
	1.75	+0.069	−0.268	−0.301	−299.385 31	−0.009 93	−299.395 24
	2.00	+0.080	−0.276	−0.304	−299.336 66	−0.010 08	−299.346 75
	2.89	+0.124	−0.303	−0.321	−299.198 73	−0.010 94	−299.209 67
	4.00	+0.085	−0.185	−0.399	−299.199 86	−0.016 41	−299.216 27
	5.00	−0.027	−0.050	−0.423	−299.267 29	−0.017 99	−299.285 28
	5.78	−0.086	+0.053	−0.467	−299.302 99	−0.021 60	−299.324 59
	6.50	−0.073	+0.089	−0.516	−299.327 67	−0.026 07	−299.353 74
	7.00	−0.043	+0.091	−0.548	−299.333 39	−0.029 30	−299.362 69
	7.50	−0.047	+0.117	−0.570	−299.329 30	−0.031 62	−299.360 92
	8.67	+0.031	+0.074	−0.605	−299.311 63	−0.036 39	−299.348 02
$^2B_1$	1.20	+0.068	−0.250	−0.318	−299.332 26	−0.011 27	−299.343 54
($n=1$)	1.35	+0.073	−0.227	−0.346	−299.404 26	−0.013 28	−299.417 54
	1.50	+0.064	−0.202	−0.362	−299.415 71	−0.014 49	−299.430 20
	1.65	+0.081	−0.163	−0.418	−299.400 64	−0.019 27	−299.419 90
	1.75	+0.096	−0.118	−0.478	−299.384 64	−0.025 15	−299.409 79
	2.00	+0.137	−0.033	−0.604	−299.351 87	−0.039 82	−299.391 69
	2.89	+0.200	−0.056	−0.644	−299.275 87	−0.044 08	−299.319 95
	4.00	+0.183	−0.008	−0.674	−299.264 57	−0.046 77	−299.311 34
	5.00	+0.089	+0.078	−0.667	−299.280 58	−0.044 78	−299.325 36
	5.78	+0.024	+0.131	−0.654	−299.297 18	−0.042 44	−299.339 61
	6.50	−0.034	+0.109	−0.575	−299.321 45	−0.032 37	−299.353 82
	7.00	−0.028	+0.097	−0.569	−299.330 62	−0.031 61	−299.362 23
	7.50	−0.040	+0.117	−0.577	−299.328 66	−0.032 47	−299.361 12
	8.67	+0.038	+0.071	−0.609	−299.312 98	−0.036 78	−299.349 76

[a] Ag_4–O_2 length is at 2.00 Å.
[b] Ag_a and Ag_b mean the inside and outside atoms in the linear Ag_4 cluster, respectively.
[c] Asterisks (*) show the results for the optimized Ag_4–O_2 distance; namely, $R_{Ag_4-O_2}$ = 1.60 and 1.90 Å for R_{O-O} = 5.78 and 7.00 Å, respectively.

Å.[12] The gross charge of the dissociated oxygen atom is calculated to be −0.98, very close to −1.0.

Table V shows the atomic charge and the partitioning of the total energy into $E^{(0)}$ and $E^{(1)}$ for the lower states of the Ag_4O_2 adcluster. Since the oxygen charges of the molecular adsorption states are smaller than those of the dissociative adsorption state, the image force terms $E^{(1)}$ of the former are smaller than those of the latter and, therefore, without the image force correction, the molecular superoxide species is more stable than the dissociative species, which does not agree with the experiment. This result again shows that the electrostatic image force correction is important for describing the oxygen adsorption on a silver surface.

The results for the O–O distances between 1.20 and 2.89 Å are shown in both Tables III and V. We see that the oxygen charges of the $^2A_1$, $^2A_2$, and $^2B_1$ states are similar to each other. For the peroxide $^2A_1$ state, the gross charge of Ag bonded directly to O_2, denoted as Ag_a, calculated with the Ag_4O_2 adcluster is similar to that calculated for the Ag_2O_2 adcluster. On the other hand, for the superoxide $^2A_2$ and $^2B_1$ states, the Ag_a charges are different between the

Ag_4O_2 and Ag_2O_2 adclusters; the former is positive, but the latter is negative. We think it natural that the Ag_a atoms bonded directly to O_2 are positively charged, which is reproduced for the larger Ag_4O_2 adcluster. Furthermore, Table V shows that the positive charges of Ag_a of the superoxide $^2A_2$ and $^2B_1$ states are smaller than those of the peroxide $^2A_1$ state in this region.

The results for the $^2A_1$ state with the Ag_4–O_2 distance fixed at 2.0 Å show that the oxygen charge tends to increase as the O–O distance is elongated. While a similar result is obtained for the $^2A_2$ state, the charge of the $^2B_1$ state is quite different. In the O–O distance of 1.20–1.65 Å, namely, in the molecular region, the oxygen charge of the $^2B_1$ state is similar to and a little larger than that of the $^2A_2$ state. In the O–O distance of 2.00–4.00 Å, namely, in the barrier region, the charge is similar to that of the $^2A_1$ state. In the O–O distance of 6.50–8.67 Å, namely, in the dissociative region, the charge is again similar to that of the $^2A_2$ state. This behavior of the oxygen charge of the $^2B_1$ state is the one which can be expected from the behavior of the potential energy curve shown in Fig. 4; the potential energy curve of the $^2B_1$ state is close to that of the $^2A_2$ state in the molecular and dissociative regions, and to that of the $^2A_1$ state in the barrier region.

In Table V, the results for the $^2A_1$ state at the optimized Ag_4–O_2 distances are also given. At the O–O distance of 5.78 Å, the optimized Ag_4–O_2 distance is 1.60 Å and the oxygen charges increase from -0.77 to -0.98 as the Ag_4–O_2 distance changes from 2.0 to 1.6 Å. The image force correction $E^{(1)}$ increases accordingly by -0.033 hartree, and the energy of the adcluster alone $E^{(0)}$ also becomes more stable by -0.038 hartree. Similar results are also obtained at the O–O distance of 7.0 Å, though the stabilizations both in $E^{(0)}$ and $E^{(1)}$ are smaller than those at 5.89 Å.

The energy barrier between the molecular and dissociative adsorption states lies at the O–O distance of 3.5 Å with the height of 71 kcal/mol. This barrier may be too high, as the barrier estimated from the Ag_2O_2 adcluster is 20 kcal/mol. One reason is probably the neglect of the correlations of the d electrons in the calculations of the Ag_4O_2 adcluster. However, the barrier of the order of 20 kcal/mol is reasonable by the following reason related to the surface structure of the Ag_4 cluster. On the Ag(110) surface illustrated in Fig. 5(a), our Ag_4 cluster and the adjacent atoms correspond to the second and first layers, respectively. Therefore, our Ag_4 cluster is incomplete for the Ag(110) surface. Upton *et al.*[18] showed that the π orbital of O_2 directed normal to the surface interacts strongly with the second layer Ag atoms, while the π orbital parallel to the surface interacts with the first layer Ag atoms. In the present study, however, the parallel π^* orbital does not have the counterpart Ag atoms and localizes on the O_2 molecule. On the other hand, on the Ag(111) surface, all the surface atoms lie on the same plane as shown in Fig. 5(b), so that this parallel Ag–O bond is thought to be much weaker than that on the Ag(110) surface. Furthermore, we expect that this parallel interaction would stabilize the transition state rather than the molecular and dissociated states, since the parallel π orbitals can interact with four Ag atoms at the same time.

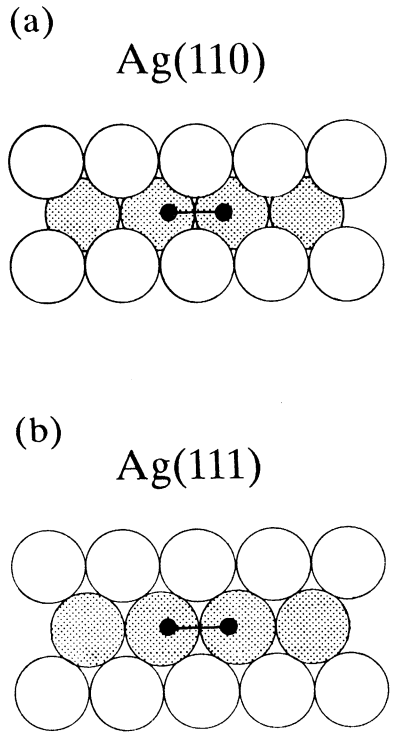

FIG. 5. Illustrations for the Ag(110) and (111) surfaces with linear Ag_4 cluster and adjacent Ag atoms. Small black filled circles show the adsorbed oxygen atoms.

In Fig. 4, the potential energy curve of the lowest $^2B_2$ state is also shown. It has two potential minima corresponding to the molecular and dissociative adsorptions. In the molecular region, the out-of-plane π MO with the symmetry b_2 is singly occupied, and the other σ, π, and π^* MOs are doubly occupied. Therefore, the bonding of this species is similar to that of the superoxide. As the O–O distance is elongated, the energy levels of the out-of-plane π and π^* MOs get closer to each other and the potential energy curve of the $^2B_2$ state becomes close to that of the $^2A_2$ state at the region longer than the O–O distance of 4 Å.

VI. ELECTRONIC STRUCTURES AND REACTIVITIES OF THE ADSORBED OXYGEN SPECIES

In this section, we discuss qualitatively the electronic structures and reactivities of the oxygen species adsorbed on the silver surface, namely, superoxide, peroxide, and dissociative species.

The orbital correlation diagram for the interaction of O_2 and Ag_2 in the Ag_2O_2 adcluster is given in Fig. 6. The left-hand side shows the active MOs of the ground state of O_2 and the right-hand side shows those of Ag_2, which consist of the $4d$ and $5s$ orbitals of Ag. The MOs of the Ag_2O_2 adcluster are given in the middle and the electron occupation shown corresponds to the $^3B_2$ state of the neutral Ag_2O_2 adcluster, though this state is with $n=0$ and is not the ground state of the interacting system. The lowest three

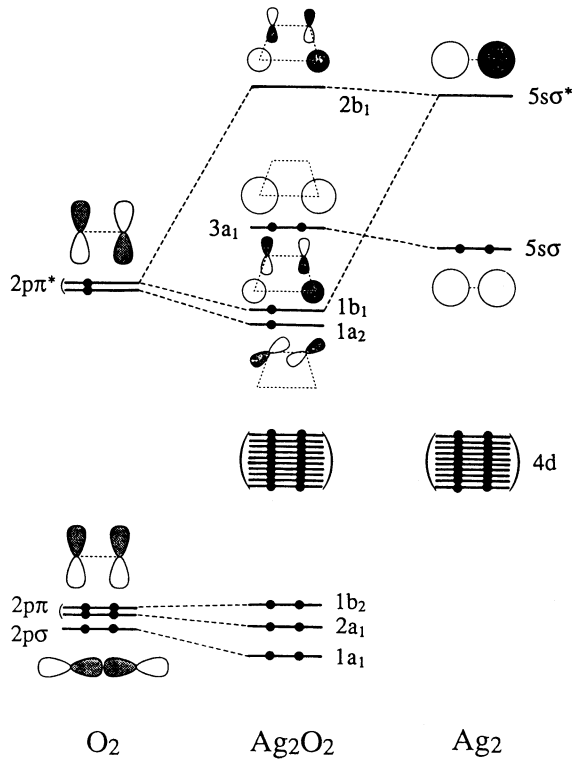

FIG. 6. A schematic orbital correlation diagram for the interaction of O_2 and Ag_2.

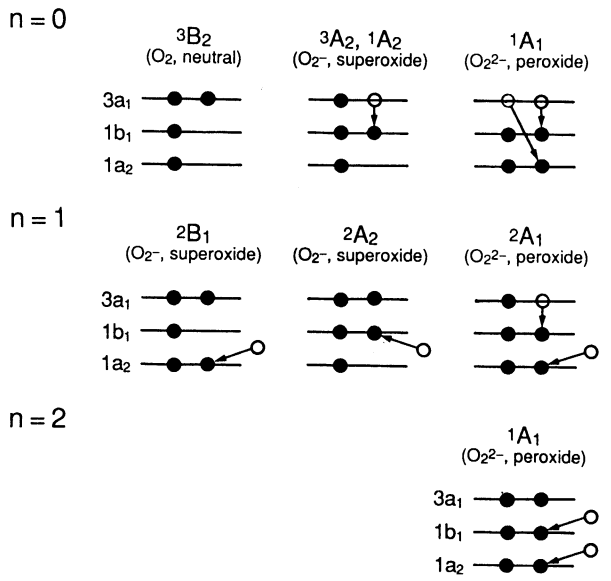

FIG. 7. Main configurations with different n for the Ag_2O_2 adcluster. The arrow shows the electron transfer, and the circles on and out of the bars show the electron holes on Ag_2 and on a bulk metal, respectively.

MOs $1a_1$, $2a_1$, and $1b_2$ of the Ag_2O_2 adcluster are essentially the bonding orbitals of O_2. The next lower ten MOs are the $4d$ orbitals of Ag and the mixing with the O_2 AOs are seemingly small. Though the roles of the $4d$ orbitals are secondary for the stabilization of the adsorbed oxygen species, they seem to play an important role for stabilizing the transition state between the molecular and dissociative adsorption states, as pointed out in the preceding section.

The main character of the $1a_2$ MO is the out-of-plane π^* orbital of O_2. The $1b_1$ MO is the result of the bonding interaction between the $5s$ σ^* MO of Ag_2 and the in-plane π^* MO of O_2, and the $2b_1$ MO is the result of the antibonding interaction between them. The $3a_1$ MO is composed mainly of the $5s$ σ MO of Ag_2. As a result, the three MOs $1a_2$, $1b_1$, and $3a_1$ seem to be important for realizing the stabilization of the adsorbed oxygen species.

The main configurations of the Ag_2O_2 adcluster with $n=0$, 1, and 2 are illustrated in Fig. 7. The arrow shows the electron transfer and the circles on and out of the bar show the electron holes on Ag_2 and on the bulk metal, respectively. The $^3B_2$ state, which is led from the ground state of the separated system Ag_2 plus O_2 has an electronic structure of $(1a_2)^1(1b_1)^1(3a_1)^2$, and the $^3A_2$ state, which corresponds to the superoxide with $n=0$, has the configuration $(1a_2)^1(1b_1)^2(3a_1)^1$. Thus, the transition from the $^3B_2$ state to the $^3A_2$ state accompanies an electron transfer from the $3a_1$ MO to the $1b_1$ MO, which is the electron transfer from Ag_2 to O_2 within the adcluster. On the other hand, the $^2A_2$ and $^2B_1$ states of the superoxide with $n=1$ have the configurations of $(1a_2)^1(1b_1)^2(3a_1)^2$ and $(1a_2)^2(1b_1)^1(3a_1)^2$, respectively. These configurations are the one-electron transferred states from the bulk metal to, respectively, the out-of-plane and in-plane orbitals of O_2. The $^2A_1$ state with $n=1$ corresponds to the peroxide which has the configuration $(1a_2)^2(1b_1)^2(3a_1)^1$. This state is produced by two electron transfers to the $1a_2$ and $1b_1$ MOs, one from the $3a_1$ MO (within the adcluster) and the other from the bulk metal. In the peroxide state described by the cluster model, namely $n=0$, two electrons are transferred from the $3a_1$ MO of Ag_2. In the peroxide state described by DAM with $n=2$, on the other hand, the two electrons are supplied from the bulk metal and the $3a_1$ MO remains doubly occupied. However, the energies of these two states with $n=0$ and 2 are higher than that of the $^2A_1$ state with $n=1$.

In the side-on geometry, the peroxide is the ground state and the superoxide is the excited state, and the energy difference between them is calculated to be 13 kcal/mol for the Ag_2O_2 adcluster. This result suggests that the superoxide in the side-on form is transformed easily into the peroxide. On the contrary, we have shown in Ref. 33 that in the end-on geometry the superoxide is the ground state and no peroxide state exists in the lower energy region. Therefore, we conclude that the transformation from superoxide to peroxide occurs in the side-on form. Furthermore, we have shown from Fig. 4 that the dissociative adsorption form is produced through the peroxide state. The dissociatively adsorbed oxygen is stabilized by the two covalent Ag–O bonds in

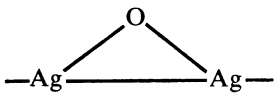

which are made by the interaction between the $5s$ orbitals

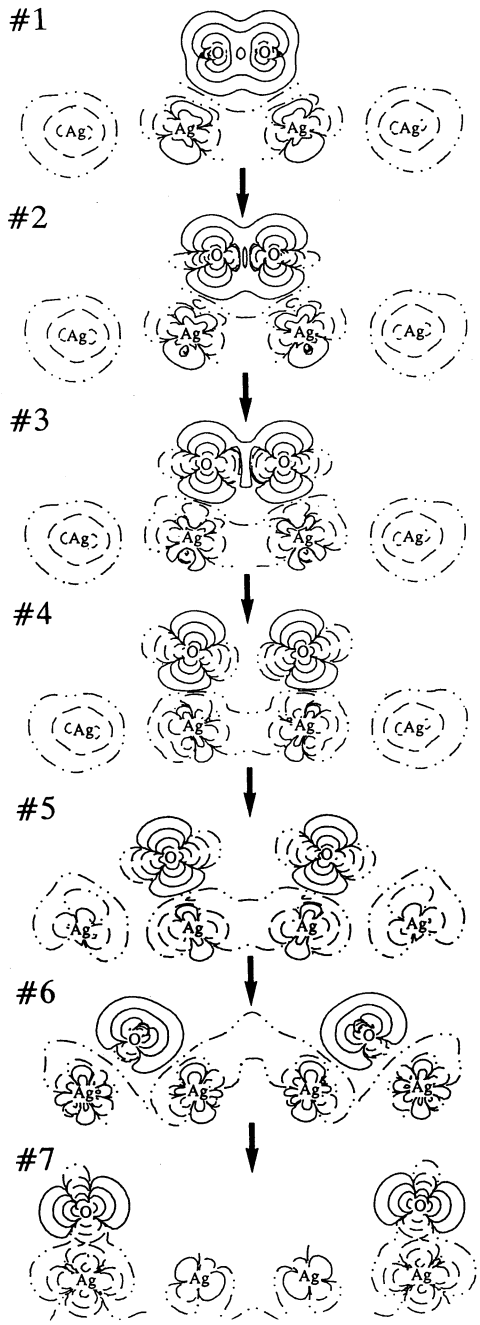

FIG. 8. Contour maps of the electron density difference of the Ag_4O_2 adcluster with $n=1$. Solid and broken lines correspond to plus and minus signs in the density difference which is defined by Eq. (2) of the text. The geometries for the positions 1–7 are defined in Table VI and correspond to the O–O distances of 1.20, 1.50, 2.00, 2.89, 4.00, 5.78, and 8.67 Å, respectively.

of Ag and the in-plane $2p$ orbitals of O, while the out-of-plane $2p$ orbital is doubly occupied and does not interact strongly with the Ag orbitals.

The change in the electron density during the molecular adsorption and the dissociation process of O_2 on an Ag_4 surface is displayed in Fig. 8. The map is defined by the electron density difference

TABLE VI. Geometry parameters of the electron density maps of the Ag_4O_2 system shown in Fig. 8.

Position	R(O–O) (Å)	R(Ag_4–O_2) (Å)
#1	1.20	2.00
#2	1.50	2.00
#3	2.00	2.00
#4	2.89	2.00
#5	4.00	2.00
#6	5.78	1.60
#7	8.67	2.00

$$\Delta\rho=\rho(Ag_4O_2^-)-\rho(Ag_4)-\rho(O)-\rho(O) \qquad (9)$$

and is given for the $^2A_1$ state, namely, from the peroxide state to the dissociated state. The density of the Ag_4 fragment is for the $^1\Sigma_g$ ground state and that of O for the ^3P ground state. Since the out-of-plane π^* orbital is localized on O_2 and doubly occupied in the $^2A_1$ state, the occupancy of the out-of-plane $2p$ orbital of O is maintained to two throughout. Two in-plane $2p$ orbitals are dealt with equivalently with the occupation number of unity.

The geometries 1–7 in Fig. 8 are defined in Table VI and correspond to the O–O distances of 1.20, 1.50, 2.00, 2.89, 4.00, 5.78, and 8.67 Å, respectively. The Ag_4–O_2 distance is fixed at 2.0 Å except for point #7, at which the optimized distance of 1.60 Å is used. The electron density at point #2 corresponds to the molecular peroxide species, and there the density of O_2 decreases in the σ-bond region and increases in the π-bond region. The density of the inside two Ag atoms are polarized toward O_2, while that of the outside two Ag atoms does not change much and decreases a little. From points #2 to #6, we see that the O–O bond is going to be completely broken. The barrier between the molecular and dissociative states lies between points #4 and #5. The O–O bond is already broken at point #4. Point #6 corresponds to the dissociative adsorption and the densities of the O atoms are inclined towards the central two Ag atoms, though the O atoms are just at the central bridge site of the two the terminal Ag_2. This inclination is therefore artificial and due to the cluster-size effect. If we neglect this inclination, we see a beautiful triangular bond between O and terminal Ag_2. Thus, the behavior of the electron density shown in Fig. 8 supports the mechanism of the molecular and dissociative adsorptions studied in this paper.

We next consider the reactivities of the adsorbed oxygen species. Figure 9 is the contour map of the frontier orbitals of the adcluster. Figures 9(a) and 9(b) are for the molecularly adsorbed superoxide species. The $^2A_2$ superoxide state has the frontier orbital in the π plane parallel to the Ag surface, and is therefore amenable for the attack from another adsorbed species (Langmuir–Hinshelwood mode). On the other hand, the $^2B_1$ superoxide has the frontier orbital extending out of the surface so that it would be reactive with molecules in a gas phase (Eley–Rideal mode). Since this orbital is antibonding between Ag and O, the electron flow into this orbital would result in a cleavage of the Ag–O bond. Furthermore, since these fron-

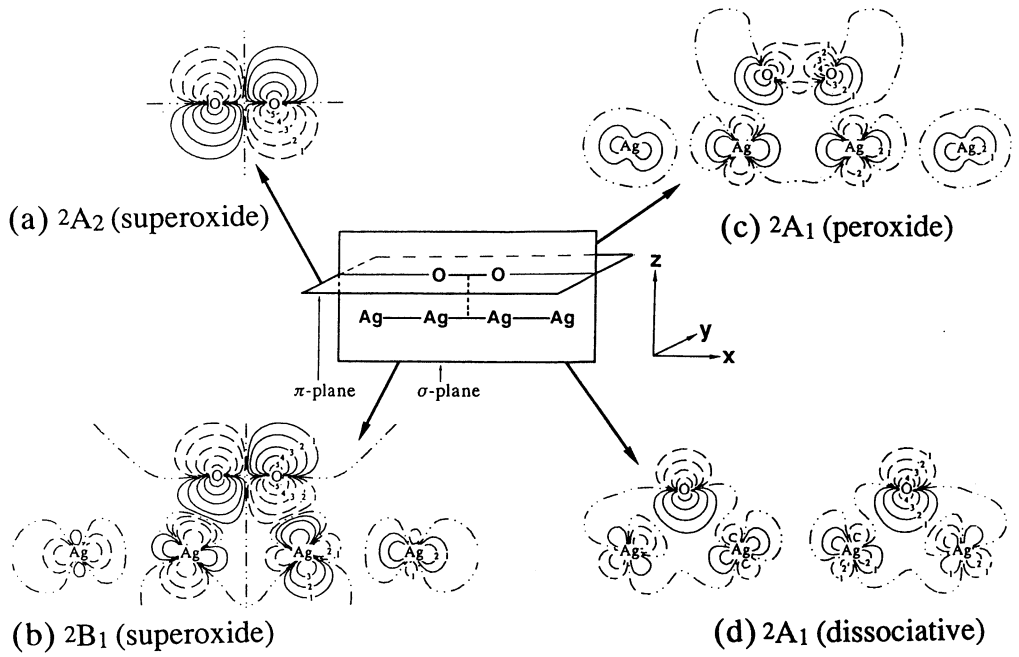

FIG. 9. Contour maps of the frontier orbitals of the Ag_4O_2 adcluster with $n=1$. Solid and broken lines correspond to plus and minus signs in the MO. Double dotted lines show the nodes of the MOs. The values of the contours are $10^{0.5}$, 10^{0}, $10^{-0.5}$, 10^{-1}, $10^{-1.5}$, and 10^{-2}, respectively.

tier MOs of the superoxides are essentially the antibonding π^* orbitals of O_2, the O–O bond will also be weakened or broken when an electron is accepted in these orbitals. In this side-on geometry, two oxygen atoms of the superoxide have the same reactivity, but those of the end-on superoxide, studied previously,[31] have different ones; namely, the outer oxygen is more reactive than the inner oxygen. Figure 9(c) is for the molecularly adsorbed peroxide species. Since this orbital is again antibonding between Ag and O, but bonding between two O atoms and between the central two Ag atoms, an electron in–out would affect the adsorption strength and the surface geometry. As shown in Sec. IV, the species leads to the dissociative adsorption state. Figure 9(d) is the singly occupied molecular orbital (SOMO) of the dissociatively adsorbed oxygen. From the extension of the frontier orbital and the gross charge on O, it is expected that this state leads to electrophilic reactions for molecules both on the surface and in a gas phase.

VII. CONCLUDING REMARKS

We have studied in this paper the chemisorption of an oxygen molecule on a Ag surface. We have been able to describe both molecular and dissociative adsorption states of O_2 by the DAM combined with the SAC/SAC-CI method. For molecular adsorption, both superoxide and peroxide species exist in the side-on geometry in contrast to the end-on geometry reported previously,[31] and the corresponding adsorption energies are calculated to be 5.5 and 17.8 kcal/mol, respectively, in comparison with the experimental value of 9.2–9.3 kcal/mol. The O–O vibrational stretching frequencies of the molecular adsorption species are in good agreement with the experimental values. The calculated O–O distances of the superoxide and the peroxide are 1.47 and 1.66 Å, respectively. The dissociative adsorption form is led from the peroxide. The stable geometry is at the bridge site (or at the threefold site) of a silver surface and the calculated Ag–O distance of 2.16 Å agrees well with the experimental value 2.06–2.17 Å. The dissociative adsorption energy is estimated to be 44.0–61.4 kcal/mol, in comparison with the observed value of 40.8–44.0 kcal/mol.

This study has shown clearly that the electron transfer from the bulk metal to the adcluster is essential for the occurrence of O_2 chemisorption on a silver surface. Electrostatic image force is also very important for stabilizing O_2 on a surface. These factors are described very naturally in the dipped adcluster model in contrast to the conventional cluster model. It is also shown that several lower electronic states are involved in the oxygen chemisorption processes. The calculation for the ground state alone is clearly insufficient. The electron transfer from the bulk metal into the adcluster, electron correlations, and the ground and excited states are calculated by the SAC/SAC-CI method. The success of the present study in describing both molecular and dissociative adsorption states with reasonable adsorption energies are due to the combined use of the DAM and the SAC/SAC-CI methods. Though the purpose of the present calculations is mostly the examination of our methodology rather than the prediction, the present results show that this method is sufficiently *a priori* to be predictive. Probably the cluster-size dependence in the DAM is also an interesting problem to be studied in the future. We believe that the size depen-

dence in the DAM should be smaller than that in the cluster model.

ACKNOWLEDGMENTS

One of the authors (H. Nakatsuji) would like to thank Mr. N. Kishimoto of Nippon Shokubai Co., Ltd. for valuable discussions in the beginning of this study. The calculations have been carried out with the FACOM M780 computer at the Data Processing Center of Kyoto University and the HITAC M-680H computer at the Institute for Molecular Science. The author thanks the IMS computer center for the grants of computing time. Part of this study has been supported by the Grant-in-Aid for Scientific Research from the Japanese Ministry of Education, Science, and Culture, and by the Kurata Foundation.

[1] D. Schmeisser, J. E. Demuth, and Ph. Avouris, Phys. Rev. B **26**, 4857 (1982).
[2] C. Pettenkofer, I. Pockrand, and A. Otto, Surf. Sci. **135**, 52 (1983); C. Pettenkofer, J. Eickmans, U. Erturk, and A. Otto, *ibid.* **151**, 9 (1985).
[3] A. Sexton and R. J. Madix, Chem. Phys. Lett. **76**, 294 (1980).
[4] C. Backx, C. P. M. deGroot, and P. Biloen, Surf. Sci. **104**, 300 (1981); Appl. Surf. Sci. **6**, 256 (1980).
[5] D. A. Outka, J. Stöhr, W. Jark, P. Stevens, J. Solomon, and R. J. Madix, Phys. Rev. B **35**, 4119 (1987); J. Stöhr and D. A. Outka, *ibid.* **36**, 7891 (1987).
[6] H. A. Engehardt, A. M. Bradshaw, and D. Menzel, Surf. Sci. **40**, 410 (1973).
[7] P. B. Clarkson and A. C. Cirillo, Jr., J. Catal. **33**, 392 (1974).
[8] M. A. Bartreau and J. Madix, Chem. Phys. Lett. **97**, 85 (1983).
[9] K. C. Prince and A. M. Bradshow, Surf. Sci. **126**, 49 (1983).
[10] C. T. Campbell, Surf. Sci. **157**, 43 (1985).
[11] K. Bange, T. E. Madey, and J. K. Sass, Chem. Phys. Lett. **113**, 56 (1985).
[12] A. Pushmann and J. Haase, Surf. Sci. **144**, 559 (1984).
[13] P. H. Krupenie, J. Phys. Chem. Ref. Data **1**, 423 (1972).
[14] L. Vaska, Acc. Chem. Res. **9**, 175 (1976).
[15] J.-H. Lin and B. J. Garrison, J. Chem. Phys. **80**, 2904 (1984).
[16] A. Selmani, J. M. Sichel, and D. R. Salahub, Surf. Sci. **157**, 208 (1985); A. Selmani, J. Andzelm, and D. R. Salahub, Int. J. Quantum Chem. **29**, 829 (1986).
[17] M. L. McKee, J. Chem. Phys. **87**, 3143 (1987).
[18] T. H. Upton, P. Stevens, and R. J. Madix, J. Chem. Phys. **88**, 3988 (1988).
[19] E. A. Carter and W. A. Goddard III, Surf. Sci. **209**, 243 (1989).
[20] K. Broomfield and R. M. Lambert, Mol. Phys. **66**, 421 (1989).
[21] P. J. van den Hoek, E. J. Baerends, and R. A. van Santen, J. Phys. Chem. **93**, 646 (1989).
[22] I. Panas, P. Siegbahn, and U. Wahlgren, J. Chem. Phys. **90**, 6791 (1989).
[23] H. Nakatsuji, J. Chem. Phys. **87**, 4995 (1987).
[24] H. Nakatsuji, H. Nakai, and Y. Fukunishi, J. Chem. Phys. **95**, 640 (1991).
[25] H. Nakatsuji, M. Hada, and T. Yonezawa, J. Am. Chem. Soc. **109**, 1902 (1987).
[26] H. Nakatsuji, Y. Matsuzaki, and T. Yonezawa, J. Chem. Phys. **88**, 5759 (1988).
[27] H. Nakatsuji and K. Hirao, J. Chem. Phys. **68**, 2035 (1978).
[28] H. Nakatsuji, Chem. Phys. Lett. **59**, 362 (1978); **67**, 329 (1979); **67**, 334 (1979).
[29] H. Nakatsuji, Acta Chimica Hungarica (in press, 1992).
[30] H. Nakatsuji and H. Nakai, Chem. Phys. Lett. **174**, 283 (1990).
[31] H. Nakatsuji and H. Nakai, Can. J. Chem. **70**, 404 (1992).
[32] L. E. Sutton, *Tables of Interatomic Distances and Configuration in Molecules and Ions* (Royal Society of Chemistry, London, 1965).
[33] P. J. Hay and W. R. Wadt, J. Chem. Phys. **82**, 270 (1985).
[34] S. Huzinaga, J. Chem. Phys. **42**, 1293 (1965).
[35] T. H. Dunning, Jr., J. Chem. Phys. **53**, 2823 (1970).
[36] T. H. Dunning, Jr. and P. J. Hay, *Modern Theoretical Chemistry*, edited by H. F. Schaeffer III (Plenum, New York, 1977), Vol. 3.
[37] K. P. Huber and G. Herzberg, *Molecular Spectra and Molecular Structure. IV. Constants of Diatomic Molecules* (Van Nostrand–Reinhold, New York, 1979).
[38] A. W. Dweydari and C. H. B. Mee, Phys. Status Solidi. A **27**, 223 (1975).
[39] J. Ho, K. M. Ervin, and W. C. Lineberger, J. Chem. Phys. **93**, 6987 (1990).
[40] H. Nakatsuji, Chem. Phys. **75**, 425 (1983).
[41] B. R. Brooks, P. Saxe, W. D. Laidig, and M. Dupuis, program system GAMESS, Program Library No. 481, Computer Center of the Institute for Molecular Science, 1981.
[42] H. Nakatsuji, program system for SAC and SAC-CI calculations, Program Library No. 146 (Y4/SAC), Data Processing Center of Kyoto University, 1985; Program Library SAC85, No. 1396, Computer Center of the Institute for Molecular Science, 1981.